Three-dimensional polarization state and spin structure of a tightly focused radially polarized Gaussian Schell-model beam

Chencheng Yan,[1] Xiangyun Li,[1] Yangjian Cai,[2,*] and Yahong Chen[1,†]

[1]*School of Physical Science and Technology, Soochow University, Suzhou 215006, China*

[2]*Shandong Provincial Engineering and Technical Center of Light Manipulation & Shandong Provincial Key Laboratory of Optics and Photonic Devices, School of Physics and Electronics, Shandong Normal University, Jinan 250014, China*

(Received 25 October 2022; accepted 15 December 2022; published 28 December 2022)

In this work, we revisit the tight focusing of a radially polarized partially coherent Gaussian Schell-model beam and examine the effect of spatial coherence of the incident beam on the focal-plane three-dimensional (3D) polarization characters, including the 3D degree of polarization, polarimetric dimensionality, and polarimetric structure. The polarimetric structure and the associated structure for the spin density vector of the tightly focused field are obtained via the 3D characteristic decomposition of the 3×3 polarization matrix. We demonstrate that the generated focused field shows the genuine 3D polarization state and a sophisticated spin structure due to the reduced spatial coherence in the incident beam. We find the contributions to whole 3D polarization state of the focused field from the pure state, middle-term state, and 3D unpolarized state in the characteristic decomposition, as well as the contributions to the total spin density vector from the spins of pure state and middle-term state can be controlled by the transverse spatial coherence width of the incident Gaussian Schell-model beam. In addition, the genuine 3D polarization and the spin structure are analyzed in the connection of the recently introduced concept of polarimetric nonregularity.

DOI: 10.1103/PhysRevA.106.063522

I. INTRODUCTION

Polarization is one of the most fundamental characteristics of light, which has played an important role in understanding the nature of light and has become a key attribute in a wide array of situations including, e.g., optical imaging, three-dimensional displays, and remote sensing [1]. Classical polarization optics usually considers the light exhibiting two-dimensional (2D) polarization states. For example, for the paraxial beams, the evolution of the electric field is always restricted to a fixed 2D plane that is orthogonal to the beam's propagation direction. In the case of paraxial beams, the 2×2 polarization matrix can be used to fully characterize the polarization properties [2]. A fundamental quality of the 2D polarization state is that its polarization matrix can be decomposed as a superposition of a fully polarized state and a 2D completely unpolarized state [3]. The state of polarization is involved in the fully polarized part, while the degree of polarization is determined by the distance between the matrices for the complete polarization state and the 2D unpolarized state.

With the rapid development of the modern nanophotonics, the extension of 2D polarization optics to the three-dimensional (3D) situation becomes significantly important [4]. This is because the light fields in the nanoscale, such as the surface waves and the tightly focused fields, are generally nonparaxial, i.e., all their three orthogonal spatial components of the field vector playing the role. A 3×3 polarization matrix was successfully used to describe the polarization properties of the 3D polarization states [5]. It is important to note that one can always find a 2D plane where the evolution of the electric field vector of a deterministic (monochromatic and fully coherent) nonparaxial structured light field at a single spatial point is restricted to [6], although the electric field vectors at different points in the space, in general, oscillate in the different planes. Contrarily, the electric field of true 3D light fluctuates in three orthogonal spatial directions at a single point in any reference frame. The polarization dimensionality of light fields can be examined with the help of the intensity anisotropy of the polarization state in the intrinsic coordinate frame [7], in which the real part of the polarization matrix is diagonalized. Three nonvanishing elements of such a diagonal matrix represent a true 3D light field.

Similar to a 2D polarization state, the polarimetric structure of a 3D polarization states is achieved by the characteristic decomposition [8]. With such a decomposition, the 3×3 polarization matrix turns into an incoherent superposition of a fully polarized (pure) state, a middle-term state, and a 3D unpolarized state. Regularly, the middle-term is regarded as a 2D unpolarized state since it is an equiprobable mixture of two uncorrelated orthogonal fully polarized states [9,10]. However, a new insight has been gained recently for the characteristic decomposition of the 3D polarization state [11,12]. It was showed that, when the polarization ellipses of the above two uncorrelated states are confined to different planes, the middle term does not describe a 2D unpolarized state but a genuine nonregular 3D polarization state. A measure for the

*yangjian_cai@163.com
†yahongchen@suda.edu.cn

nonregularity of the 3D polarization state is provided by the definition of the degree of nonregularity [13].

Meanwhile, the spin angular momentum (SAM) is another intriguing characteristic of light [14], which has gained wide interest in photonics [15–18]. The SAM is associated with the circular polarization state in a light field. For a regular 3D polarization state, the SAM is carried only by the pure state, as the middle-term state (now is a 2D unpolarized state) and the 3D unpolarized state carry no spin. However, for a nonregular 3D state, a distinguishing physical property is that the middle-term state always carries a nonzero spin as the polarization matrix for this state is now a complex matrix and the degree of circular polarization is present [19]. As a result, the total SAM of a nonregular 3D polarization state is generally given as a vector sum of those of the pure state and the middle-term state.

The genuine 3D polarization state exists only in the random light fields with the field components being partially correlated [7,20]. For example, it was demonstrated only recently that any random evanescent wave created in total internal reflection of a partially polarized or 2D unpolarized planar field is in a 3D and nonregular polarization state [21]. The purely transverse spin in the partially polarized evanescent wave observed quite recently in experiment [22] is due to its true nonregular 3D nature. It was shown that the random light field generated by tight focusing of a partially polarized 2D planar wave also possesses genuine 3D polarization and exhibits high degree of nonregularity [23], and therefore, the random focused field is endowed with rich internal spin structure [24].

On the other hand, it was demonstrated that, when a fully polarized, but spatially partially coherent beam is taken to be the incident beam for the tight focusing system, the partial correlations will also be induced within the orthogonal field components of the focused field at a single point [25], indicating that the true 3D polarization state in the random focused field generated by spatially partially coherent beam is possible. A recent study has shown that the tightly focused radially polarized Gaussian Schell-model beam indeed exhibits the 3D nonregular polarization character [23]. However, how will the associated spin density vector of the middle-term state affect the total spin in the focused field and what is the role of the spatial coherence on the 3D polarization characters and the spin structures have not yet been addressed.

To this end, in this work, we revisit the tight focusing of a radially polarized Gaussian Schell-model beam [26] with the help of the recently developed convolution approach for fast calculation of the tightly focused partially coherent vectorial Schell-model beams [27]. We focus on the effect of two-point spatial coherence of incident beam on the 3D polarization properties of the focused field by examining the 3D degree of polarization, polarization dimensionality, 3D characteristic decomposition, polarimetric nonregularity, and spin structure of the 3D polarization state.

This work is organized as follows. In Sec. II we recall the theoretical background for the genuine 3D polarization state. In Sec. III, we introduce the fast calculation method for the tight focusing of an electromagnetic partially coherent Schell-model beam. In Sec. IV, we present the simulation results and discuss the behavior of the polarimetric quantities in the focal plane for the tightly focused radially polarized Gaussian Schell-model beam. Section V summarizes the main findings of this work.

II. THEORETICAL BACKGROUND

We consider a random, but statistically stationary, three-component electromagnetic field. The (second-order) statistical properties of such a field in the space-frequency domain are involved in a 3×3 cross-spectral density matrix [28]

$$\mathbf{W}(\mathbf{r}_1, \mathbf{r}_2) = \langle \mathbf{E}^*(\mathbf{r}_1)\mathbf{E}^{\mathrm{T}}(\mathbf{r}_2)\rangle, \tag{1}$$

where $\mathbf{r}_1$ and $\mathbf{r}_2$ are two arbitrary spatial points, $\mathbf{E}(\mathbf{r}) = [E_1(\mathbf{r}), E_2(\mathbf{r}), E_3(\mathbf{r})]^{\mathrm{T}}$ are the three-component random field realization vector with $E_1(\mathbf{r})$, $E_2(\mathbf{r})$, and $E_3(\mathbf{r})$ being the field components in the Cartesian coordinates along x, y, and z directions, respectively. The asterisk, superscript T, and the angle brackets denote the complex conjugate, matrix transpose, and ensemble average, respectively. The polarization properties of such a random field can be characterized by a 3×3 polarization matrix, which is fully specified by the single-point value of the cross-spectral density matrix, i.e.,

$$\mathbf{\Phi}(\mathbf{r}) = \mathbf{W}(\mathbf{r}, \mathbf{r}). \tag{2}$$

The polarization matrix $\mathbf{\Phi}(\mathbf{r})$ is Hermitian and satisfies the nonnegative definiteness conditions [5]. Thus, the polarization matrix can be decomposed as $\mathbf{\Phi}(\mathbf{r}) = \mathbf{\Phi}'(\mathbf{r}) + i\mathbf{\Phi}''(\mathbf{r})$, where the prime and double prime denote the real and imaginary parts, respectively. The real part matrix $\mathbf{\Phi}'(\mathbf{r})$ is a symmetric and positive semi-definite matrix, while the imaginary part matrix $\mathbf{\Phi}''(\mathbf{r})$ is skew symmetric [5]. The polarization matrix has three nonnegative eigenvalues $\lambda_1 \geqslant \lambda_2 \geqslant \lambda_3$ and the corresponding eigenvectors are expressed as $\hat{\mathbf{u}}_1$, $\hat{\mathbf{u}}_2$, and $\hat{\mathbf{u}}_3$, respectively. The three eigenvectors are the orthonormal and column vectors.

A. Polarization dimensionality

To see the polarization dimensionality of the random field, the polarization matrix $\mathbf{\Phi}(\mathbf{r})$ is rotated into the intrinsic coordinate frame with an orthogonal transformation matrix $\mathbf{Q}_0$. Here, $\mathbf{Q}_0$ is a 3×3 matrix which obeys $\mathbf{Q}_0^{\mathrm{T}} = \mathbf{Q}_0^{-1}$ and $\det\mathbf{Q}_0 = 1$. We note that the physical polarization properties of the field do not change under such orthogonal transformation. In the intrinsic coordinate frame, the polarization matrix becomes [7]

$$\mathbf{\Phi}_0(\mathbf{r}) = \mathbf{Q}_0^{\mathrm{T}}\mathbf{\Phi}(\mathbf{r})\mathbf{Q}_0 = \mathbf{\Phi}_0'(\mathbf{r}) + i\mathbf{\Phi}_0''(\mathbf{r}), \tag{3}$$

where

$$\mathbf{\Phi}_0'(\mathbf{r}) = \begin{pmatrix} a_1 & 0 & 0 \\ 0 & a_2 & 0 \\ 0 & 0 & a_3 \end{pmatrix}, \tag{4}$$

$$\mathbf{\Phi}_0''(\mathbf{r}) = \begin{pmatrix} 0 & -n_3 & n_2 \\ n_3 & 0 & -n_1 \\ -n_2 & n_1 & 0 \end{pmatrix}. \tag{5}$$

The real part $\mathbf{\Phi}_0'(\mathbf{r})$ is a diagonal matrix with the elements $a_1 \geqslant a_2 \geqslant a_3 \geqslant 0$ being the three eigenvalues of $\mathbf{\Phi}'(\mathbf{r})$. The elements in the imaginary part $\mathbf{\Phi}_0''(\mathbf{r})$ form the angular-momentum vector $\mathbf{n} = 2(n_1, n_2, n_3)$ of the state with

the factor of 2 confirming the bosonic nature of photons [11,29,30]. The eigenvalues a_1, a_2, and a_3 are the principal intensities, which constitute the total intensity $I = a_1 + a_2 + a_3$ of the state $\mathbf{\Phi}(\mathbf{r})$. For the principal intensities $a_1 > 0$, $a_2 = 0$, and $a_3 = 0$, it is found that the electric field fluctuates only in a single direction and thus the field is regarded as one-dimensional (1D) light. In the case when only $a_3 = 0$, the field oscillation is restricted to a plane and the light is considered as 2D light. When all three eigenvalues are positive, the intensity of each Cartesian field component is nonzero for any orientation of the frame. Thus, the field fluctuates in all three dimensions and is considered as 3D.

To characterize the dimensionality of the light field more quantitatively, one may adopt the definition of polarimetric dimension [7]

$$D(\mathbf{r}) = 3 - 2d(\mathbf{r}), \tag{6}$$

where $d(\mathbf{r})$ is the distance between the real-valued matrix $\mathbf{\Phi}'(\mathbf{r})$ and the 3×3 identity matrix (corresponding to the intensity-isotropic 3D light), i.e.,

$$d(\mathbf{r}) = \sqrt{\frac{3}{2}\left[\frac{\mathrm{tr}\mathbf{\Phi}'^2(\mathbf{r})}{\mathrm{tr}^2\mathbf{\Phi}'(\mathbf{r})} - \frac{1}{3}\right]}. \tag{7}$$

The quantity $d(\mathbf{r})$ describes the degree of intensity anisotropy of the polarization state $\mathbf{\Phi}(\mathbf{r})$ and is bounded as $0 \leqslant d(\mathbf{r}) \leqslant 1$. The polarimetric dimension, therefore, obeys $1 \leqslant D(\mathbf{r}) \leqslant 3$ with the upper and lower limits corresponding to the 1D light and the intensity-isotropic 3D (unpolarized) light, respectively. It is remarkable that the polarimetric dimension remains invariant under coordinate rotations since the rotations do not change the polarization state. Thus, the polarimetric dimension can also be written in terms of the eigenvalues of $\mathbf{\Phi}'(\mathbf{r})$, i.e.,

$$D(\mathbf{r}) = 3 - \frac{\sqrt{2[(a_1 - a_2)^2 + (a_1 - a_3)^2 + (a_2 - a_3)^2]}}{a_1 + a_2 + a_3}. \tag{8}$$

We note that only for $a_1 > 0$, $a_2 = a_3 = 0$ (1D light), $D(\mathbf{r}) = 1$. For the 2D light ($a_1 \geqslant a_2 > 0$ and $a_3 = 0$), $1 < D(\mathbf{r}) \leqslant 2$. For $2 < D(\mathbf{r}) \leqslant 3$, the light field is essentially 3D as the three orthogonal components have nonzero intensity for any orientation of the Cartesian reference frame. It is noted here that, for $1 < D(\mathbf{r}) \leqslant 2$, the light can also be 3D if the intensity distribution is anisotropic.

B. Characteristic decomposition

To show more intuitively the polarimetric structure of the 3D polarization state, we decompose the 3×3 polarization matrix with the characteristic decomposition, i.e., the 3×3 polarization matrix is decomposed as an incoherent superposition of three polarization matrices with particular interpretations [8]

$$\mathbf{\Phi} = I[P_1\hat{\mathbf{\Phi}}_p + (P_2 - P_1)\hat{\mathbf{\Phi}}_m + (1 - P_2)\hat{\mathbf{\Phi}}_u], \tag{9}$$

where $I = \lambda_1 + \lambda_2 + \lambda_3$ is the total intensity with λ_1, λ_2, and λ_3 being the nonnegative eigenvalues of $\mathbf{\Phi}$, as before. The parameters P_1 and P_2 are the indices of polarimetric purity, which can be obtained by

$$P_1 = (\lambda_1 - \lambda_2)/I, \tag{10}$$

$$P_2 = 1 - 3\lambda_3/I, \tag{11}$$

and they obey $0 \leqslant P_1 \leqslant P_2 \leqslant 1$. The three polarization matrices are expressed as

$$\hat{\mathbf{\Phi}}_p = \hat{\mathbf{u}}_1\hat{\mathbf{u}}_1^\dagger, \tag{12}$$

$$\hat{\mathbf{\Phi}}_m = \tfrac{1}{2}(\hat{\mathbf{u}}_1\hat{\mathbf{u}}_1^\dagger + \hat{\mathbf{u}}_2\hat{\mathbf{u}}_2^\dagger), \tag{13}$$

$$\hat{\mathbf{\Phi}}_u = \tfrac{1}{3}(\hat{\mathbf{u}}_1\hat{\mathbf{u}}_1^\dagger + \hat{\mathbf{u}}_2\hat{\mathbf{u}}_2^\dagger + \hat{\mathbf{u}}_3\hat{\mathbf{u}}_3^\dagger), \tag{14}$$

where $\hat{\mathbf{u}}_1$, $\hat{\mathbf{u}}_2$, and $\hat{\mathbf{u}}_3$ are the eigenvectors of the polarization matrix $\mathbf{\Phi}$ corresponding to the eigenvalues λ_1, λ_2, and λ_3, respectively. It is obvious that the first polarization matrix $\hat{\mathbf{\Phi}}_p$ describes a fully polarized (pure) state with its polarimetric dimension bounded as $1 \leqslant D \leqslant 2$. The last polarization matrix $\hat{\mathbf{\Phi}}_u = \mathbf{I}/3$, with $\mathbf{I}$ being the 3×3 identity matrix, denotes a 3D completely unpolarized field with its polarimetric dimension $D = 3$.

However, the physical interpretation of the middle-term state $\hat{\mathbf{\Phi}}_m$ requires more attention. Traditionally, the middle term is regarded as a 2D unpolarized light (with polarimetric dimension $D = 2$) since the matrix is composed by two uncorrelated orthonormal states $\hat{\mathbf{u}}_1$ and $\hat{\mathbf{u}}_2$. This is true when the polarization ellipses of the two states lie in the same plane. However, when the middle term $\hat{\mathbf{\Phi}}_m$ corresponds to an incoherent mixture of two equal-intensity states whose polarization ellipses are confined to different planes, the polarization state $\hat{\mathbf{\Phi}}_m$ does not describe 2D unpolarized light but genuine 3D light [12]. In such a case (excluding the special case $P_2 - P_1 = 0$), the polarization state is named as the nonregular 3D polarization state. The polarimetric dimension for the nonregular state $\hat{\mathbf{\Phi}}_m$ is bounded as $2 < D \leqslant 5/2$ (shown below) with the upper limit corresponding to the perfectly nonregular state, i.e., the state $\hat{\mathbf{\Phi}}_m$ is an equiprobable mixture of a circularly polarized state and a mutually orthogonal linearly polarized state.

A measure for the nonregularity of the state $\hat{\mathbf{\Phi}}_m$ is provided by the degree of nonregularity [13]

$$P_N(\hat{\mathbf{\Phi}}_m) = 4\hat{m}_3, \tag{15}$$

where $0 \leqslant \hat{m}_3 \leqslant 1/4$ is the smallest eigenvalue of the real part of $\hat{\mathbf{\Phi}}_m$. The degree of nonregularity $P_N(\hat{\mathbf{\Phi}}_m)$ is bounded between 0 and 1, with the lower and upper limits corresponding to a regular and a perfectly nonregular state. The degree of nonregularity and polarimetric dimension of $\hat{\mathbf{\Phi}}_m$ are related as [13]

$$D(\hat{\mathbf{\Phi}}_m) = 3 - \sqrt{1 - 3P_N(\hat{\mathbf{\Phi}}_m)[2 - P_N(\hat{\mathbf{\Phi}}_m)]/4}. \tag{16}$$

As shown in Eq. (16) when the polarization state is nonregular, i.e., $0 < P_N(\hat{\mathbf{\Phi}}_m) \leqslant 1$, the polarimetric dimension obeys $2 < D(\hat{\mathbf{\Phi}}_m) \leqslant 5/2$ indicating the true 3D character. Considering the weight of $\hat{\mathbf{\Phi}}_m$ in the characteristic decomposition, the degree of nonregularity of the full state $\mathbf{\Phi}$ is given by

$$P_N = (P_2 - P_1)P_N(\hat{\mathbf{\Phi}}_m), \tag{17}$$

which is also bounded between 0 and 1. When $P_N = 1$, the whole state $\mathbf{\Phi} = I\hat{\mathbf{\Phi}}_m$ with $P_N(\hat{\mathbf{\Phi}}_m) = 1$, indicating that not only the middle-term state but also the whole polarization state $\mathbf{\Phi}$ itself is perfectly nonregular.

From the above characteristic decomposition, it is found that 3D nature of a light field is from not only the 3D unpolarized state but also the 3D nonregular state, which, however, is normally regarded as a 2D unpolarized state. The degree of polarization for the 3D light field can be characterized by the distance between the polarization matrix $\mathbf{\Phi}(\mathbf{r})$ and the polarization matrix $\mathbf{I}$ for the completely 3D unpolarized light [31], i.e.,

$$P_{3D}(\mathbf{r}) = \sqrt{\frac{3}{2}\left[\frac{\mathrm{tr}\mathbf{\Phi}^2(\mathbf{r})}{\mathrm{tr}^2\mathbf{\Phi}(\mathbf{r})} - \frac{1}{3}\right]}. \tag{18}$$

$P_{3D}(\mathbf{r}) = 0$ denotes that polarization matrix $\mathbf{\Phi}(\mathbf{r})$ is proportional to a 3×3 identity matrix and the state is a fully 3D unpolarized state. For $P_{3D}(\mathbf{r}) = 1$, the field is fully polarized with its polarimetric dimension fixed in the range $1 \leqslant D \leqslant 2$. Furthermore, it was proved that, for $P_{3D}(\mathbf{r}) < 0.5$, the field is genuinely 3D. This is because for a 2D field, its smallest degree of polarization is $P_{3D}(\mathbf{r}) = 0.5$ when the field is a 2D unpolarized light. The degree of polarization can also by characterized by the polarimetric purity by taking into account all the contributions of the degrees of linear polarization and circular polarization as well as the degree of directionality in the pure state $\hat{\mathbf{\Phi}}_p$ and in the nonregular polarization state $\hat{\mathbf{\Phi}}_m$, i.e., the 3D degree of polarization can be written in terms of the indices of polarimetric purity P_1 and P_2 as [12,32]

$$P_{3D} = \frac{1}{2}\sqrt{3P_1^2 + P_2^2}. \tag{19}$$

C. Spin structure

The spin angular momentum (SAM) of light is closely related to the degree of circular polarization. In view of the traditional characteristic decomposition, the SAM of a 3D light field is determined solely by the pure state (first term in the decomposition) since the middle term and the last term denote the 2D unpolarized and 3D unpolarized states, respectively, with both states lacking the degree of circular polarization. However, when the middle-term state in the characteristic decomposition is a nonregular state, the degree of circular polarization is nonzero. As a result, the SAM of the 3D light is involved not only in the pure state, but also in the nonregular state. The total spin density vector of the polarization state $\mathbf{\Phi}$ thus can be expressed as [19]

$$\mathbf{s} = \mathbf{s}_p + \mathbf{s}_m = IP_1\hat{\mathbf{n}}_p + I(P_2 - P_1)\hat{\mathbf{n}}_m, \tag{20}$$

where $\hat{\mathbf{n}}_p$ and $\hat{\mathbf{n}}_m$ are the spin density vectors for the states $\hat{\mathbf{\Phi}}_p$ and $\hat{\mathbf{\Phi}}_m$, respectively. The spin density vector $\hat{\mathbf{n}}_p$ of the pure state $\hat{\mathbf{\Phi}}_p$ is orthogonal to the plane containing the polarization ellipse of the state $\hat{\mathbf{u}}_1$ and can be obtained by the imaginary part of $\hat{\mathbf{\Phi}}_p$, i.e., the imaginary part is of the form

$$\hat{\mathbf{\Phi}}_p'' = \frac{1}{2}\begin{pmatrix} 0 & \hat{n}_{p3} & -\hat{n}_{p2} \\ -\hat{n}_{p3} & 0 & \hat{n}_{p1} \\ \hat{n}_{p2} & -\hat{n}_{p1} & 0 \end{pmatrix}. \tag{21}$$

The related spin density vector is [19,29]

$$\hat{\mathbf{n}}_p = (\hat{n}_{p1}, \hat{n}_{p2}, \hat{n}_{p3}). \tag{22}$$

As shown in Eq. (13), the spin density vector $\hat{\mathbf{n}}_m$ for the nonregular state $\hat{\mathbf{\Phi}}_m$ is determined by both the states $\hat{\mathbf{u}}_1$ and $\hat{\mathbf{u}}_2$, i.e.,

$$\hat{\mathbf{n}}_m = \tfrac{1}{2}(\hat{\mathbf{n}}_1 + \hat{\mathbf{n}}_2), \tag{23}$$

where the spin density vector $\hat{\mathbf{n}}_1 = \hat{\mathbf{n}}_p$ for $\hat{\mathbf{u}}_1$, and the spin density vector $\hat{\mathbf{n}}_2$ for the state $\hat{\mathbf{u}}_2$ can be obtained by extracting the imaginary part of the polarization matrix $\hat{\mathbf{u}}_2\hat{\mathbf{u}}_2^\dagger$ with the similar fashion shown in Eq. (21). Since the spin $\hat{\mathbf{n}}_m$ does not vanish only when the field is nonregular, its value is connected with the degree of nonregularity of the nonregular polarization state by [13,19]

$$P_N(\hat{\mathbf{\Phi}}_m) = 1 - \sqrt{1 - 4|\hat{\mathbf{n}}_m|^2}. \tag{24}$$

The middle component necessarily has nonzero spin when $P_N(\hat{\mathbf{\Phi}}_m) > 0$. The length of the spin density vector reaches its maximum value $|\hat{\mathbf{n}}_m| = 1/2$ when the middle component is a perfectly nonregular state $[P_N(\hat{\mathbf{\Phi}}_m) = 1]$. Remarkably, the total spin density vector obtained from the characteristic decomposition coincides with that obtained by averaging over the spins of the monochromatic field realizations, i.e., $\mathbf{s} = \langle \mathbf{E}^* \times \mathbf{E} \rangle''$ (double prime denotes the imaginary part).

III. TIGHT FOCUSING OF ELECTROMAGNETIC SCHELL-MODEL BEAM

In this work, we aim to examine the 3D polarization characters, including the 3D degree of polarization, polarization dimensionality, polarimetric nonregularity, and spin structure of a tightly focused electromagnetic Gaussian Schell-model beam with the help of the general theory presented above. We consider that the incident beam of the tight focusing system is a statistically stationary, partially coherent beam-like vector field that propagates along, say, the z axis. The cross-spectral density of such beam can be characterized by a 2×2 matrix [28]

$$\mathbf{W}^{(0)}(\boldsymbol{\rho}_1, \boldsymbol{\rho}_2) = \begin{bmatrix} W_{11}^{(0)}(\boldsymbol{\rho}_1, \boldsymbol{\rho}_2) & W_{12}^{(0)}(\boldsymbol{\rho}_1, \boldsymbol{\rho}_2) \\ W_{21}^{(0)}(\boldsymbol{\rho}_1, \boldsymbol{\rho}_2) & W_{22}^{(0)}(\boldsymbol{\rho}_1, \boldsymbol{\rho}_2) \end{bmatrix}, \tag{25}$$

where the elements $W_{\alpha\beta}^{(0)}(\boldsymbol{\rho}_1, \boldsymbol{\rho}_2) = \langle E_\alpha^{(0)*}(\boldsymbol{\rho}_1) E_\beta^{(0)}(\boldsymbol{\rho}_2) \rangle$, $(\alpha, \beta) = (1, 2)$ with the superscript (0) denoting the input plane, $\boldsymbol{\rho}_1 = (\rho_{1x}, \rho_{1y})$ and $\boldsymbol{\rho}_2 = (\rho_{2x}, \rho_{2y})$ being two arbitrary transverse spatial positions in the input plane, and $[E_1^{(0)}(\boldsymbol{\rho}), E_2^{(0)}(\boldsymbol{\rho})]$ being the components of the field realization vector $\mathbf{E}^{(0)}(\boldsymbol{\rho})$ along the x and y directions, respectively. For the partially coherent vector beams with Schell-model-type correlation functions, the elements in the cross-spectral density matrix can be expressed as [2]

$$W_{\alpha\beta}^{(0)}(\boldsymbol{\rho}_1, \boldsymbol{\rho}_2) = \mathcal{A}_\alpha^*(\boldsymbol{\rho}_1)\mathcal{A}_\beta(\boldsymbol{\rho}_2)\mu_{\alpha\beta}(\boldsymbol{\rho}_1 - \boldsymbol{\rho}_2), \tag{26}$$

where $\mathcal{A}_1(\boldsymbol{\rho})$ and $\mathcal{A}_2(\boldsymbol{\rho})$ are the (complex) amplitudes of the field components along the x and y directions, respectively,

which determines the initial polarization properties of the incident beam; $\mu_{\alpha\beta}(\boldsymbol{\rho}_1 - \boldsymbol{\rho}_2)$ is the normalized correlation function among the field components along the α and β directions. We note that for the Schell-model-type partially coherent beam, the correlation functions depend only on the position difference.

It is considered that the tight focusing system is an aplanatic objective lens that obeys the sine condition. The transmission of light through such a lens can be treated within the ray picture. The incident rays are refracted at the reference sphere whose radius equals the focal distance f of the lens. After transmitted through the sphere, the polarization state of the incident beam changes. In the basis of the spherical coordinate, the radial polarization vector tilts at the off-axial points and acquires a longitudinal component, i.e., the transmitted radial polarization vector changes from $\hat{\mathbf{e}}_r = \cos\phi\hat{\mathbf{e}}_x + \sin\phi\hat{\mathbf{e}}_y$ to $\hat{\mathbf{e}}_r^{(\mathrm{t})} = \cos\theta\hat{\mathbf{e}}_r + \sin\theta\hat{\mathbf{e}}_z$, while the transmitted azimuthal polarization vector remains unchanged, i.e., $\hat{\mathbf{e}}_\phi^{(\mathrm{t})} = \hat{\mathbf{e}}_\phi$ with $\hat{\mathbf{e}}_\phi = -\sin\phi\hat{\mathbf{e}}_x + \cos\phi\hat{\mathbf{e}}_y$. Above, $\hat{\mathbf{e}}_x$, $\hat{\mathbf{e}}_y$, and $\hat{\mathbf{e}}_z$ are the Cartesian unit vectors along the x, y, and z directions, respectively; $0 \leqslant \phi < 2\pi$ is the azimuthal angle with respect to the x axis, θ is the angle formed by a ray emanating from the reference sphere and the z axis, which is bounded between 0 and $\theta_{\max} = \arcsin(\mathrm{NA}/n_t)$ with NA being the numerical aperture of the objective lens and n_t being the refractive index of the medium after the lens. A point on the reference sphere can be expressed in terms of the angles ϕ and θ. The transverse spatial position vector of the beam in the input plane can also be written in terms of the angles via $\boldsymbol{\rho} = (f\cos\phi\sin\theta, f\sin\phi\sin\theta)$. By transforming the polarization unit vectors in the spherical coordinate into the Cartesian coordinate, we obtain that the transmitted field realization vector through the reference sphere can be expressed as

$$\mathbf{E}^{(\mathrm{t})}(\phi,\theta) = P(\theta)\mathbf{E}^{(0)}(\boldsymbol{\rho})\mathbf{N}(\phi,\theta), \tag{27}$$

where $P(\theta)$ is the apodization function of the objective lens. For the lens obeying the sine condition, we have $P(\theta) = \sqrt{\cos\theta}$, according to the power conservation requirement during the transmission of light through the lens. The transform matrix $\mathbf{N}(\phi,\theta)$ in the Cartesian coordinate is written as

$$\mathbf{N}(\phi,\theta) = \begin{pmatrix} \sin^2\phi + \cos^2\phi\cos\theta & \sin\phi\cos\phi(\cos\theta - 1) & \cos\phi\sin\theta \\ \sin\phi\cos\phi(\cos\theta - 1) & \cos^2\phi + \sin^2\phi\cos\theta & \sin\phi\sin\theta \end{pmatrix}, \tag{28}$$

which is 2×3 normalized matrix that transforms the two-component field vector to the three-component field vector.

Based on the Richards-Wolf's method [33], the electric field in the focal region is given by the vectorial diffraction integral of the field over the reference spherical surface. Thus, the field realization vector near the focal region is obtained by

$$\mathbf{E}(\mathbf{r},z) = -\frac{if}{\lambda}\int_0^{2\pi}\int_0^{2\pi} T(\phi,\theta)\mathbf{E}^{(\mathrm{t})}(\phi,\theta)e^{i(k_z z - k_x x - k_y y)}\sin\theta d\theta d\phi, \tag{29}$$

where $\mathbf{r} = (x, y)$ is the transverse position vector in the plane of distance z from the focus, and $T(\phi,\theta)$ is a truncation function with its value $T(\phi,\theta) = 1$ in the region where $\mathbf{E}^{(\mathrm{t})}(\phi,\theta)$ differs from zero and vanishes in the region where $\mathbf{E}^{(\mathrm{t})}(\phi,\theta) = 0$. The components of the wave vector $\mathbf{k}$ are expressed as $k_x = -k\cos\phi\sin\theta$, $k_y = -k\sin\phi\sin\theta$, and $k_z = k\cos\theta$ with $k = 2\pi n_t/\lambda$. By using the relation $\boldsymbol{\rho} = (f\cos\phi\sin\theta, f\sin\phi\sin\theta)$, the above integral can be written as

$$\mathbf{E}(\mathbf{r},z) = -\frac{i}{\lambda f}\iint_{-\infty}^{+\infty}\frac{T(\boldsymbol{\rho})}{\sqrt{1-\boldsymbol{\rho}^2/f^2}}\mathbf{E}^{(\mathrm{t})}(\boldsymbol{\rho})e^{ik(\boldsymbol{\rho}\cdot\mathbf{r})/f}e^{ik\sqrt{1-\boldsymbol{\rho}^2/f^2}z}d^2\boldsymbol{\rho}. \tag{30}$$

We now take all the field realizations into account. The 3×3 coherence matrix near the focal region at z is therefore expressed as

$$\begin{aligned} W_{ij}(\mathbf{r}_1,\mathbf{r}_2,z) = {} & \frac{1}{\lambda^2 f^2}\sum_{\alpha=1}^{2}\sum_{\beta=1}^{2}\iint_{-\infty}^{+\infty}\iint_{-\infty}^{+\infty}\frac{T(\boldsymbol{\rho}_1)T(\boldsymbol{\rho}_2)}{(1-\boldsymbol{\rho}_1^2/f^2)^{1/4}(1-\boldsymbol{\rho}_2^2/f^2)^{1/4}}e^{-ik(\boldsymbol{\rho}_1\cdot\mathbf{r}_1 - \boldsymbol{\rho}_2\cdot\mathbf{r}_2)/f} \\ & \times e^{-ikz(\sqrt{1-\boldsymbol{\rho}_1^2/f^2}-\sqrt{1-\boldsymbol{\rho}_2^2/f^2})}N_{\alpha i}^*(\boldsymbol{\rho}_1)N_{\beta j}(\boldsymbol{\rho}_2)W_{\alpha\beta}^{(0)}(\boldsymbol{\rho}_1,\boldsymbol{\rho}_2)d^2\boldsymbol{\rho}_1 d^2\boldsymbol{\rho}_2, \end{aligned} \tag{31}$$

where $(i, j) = (1, 2, 3)$, $N_{\alpha i}(\boldsymbol{\rho})$ and $N_{\beta j}(\boldsymbol{\rho})$ denote the elements in the transform matrix $\mathbf{N}(\boldsymbol{\rho})$, and $W_{\alpha\beta}^{(0)}(\boldsymbol{\rho}_1,\boldsymbol{\rho}_2)$ is the element of the cross-spectral density matrix for the incident beam. By using the relation of Schell-model correlation in Eq. (26) and introducing the function $A_{\alpha i}(\boldsymbol{\rho},z) = e^{ikz\sqrt{1-\boldsymbol{\rho}^2/f^2}}T(\boldsymbol{\rho})N_{\alpha i}(\boldsymbol{\rho})\mathcal{A}_\alpha(\boldsymbol{\rho})/(1-\boldsymbol{\rho}^2/f^2)^{1/4}$, the 3×3 coherence matrix can be rewritten as

$$W_{ij}(\mathbf{r}_1,\mathbf{r}_2,z) = \frac{1}{\lambda^2 f^2}\sum_{\alpha=1}^{2}\sum_{\beta=1}^{2}\iint A_{\alpha i}^*(\boldsymbol{\rho}_1,z)A_{\beta j}(\boldsymbol{\rho}_2,z)e^{-ik(\boldsymbol{\rho}_1\cdot\mathbf{r}_1 - \boldsymbol{\rho}_2\cdot\mathbf{r}_2)/f}\mu_{\alpha\beta}(\boldsymbol{\rho}_1 - \boldsymbol{\rho}_2)d^2\boldsymbol{\rho}_1 d^2\boldsymbol{\rho}_2. \tag{32}$$

The above integrals can be reduced to

$$W_{ij}(\mathbf{r}_s,\mathbf{r}_d,z) = \frac{1}{\lambda^4 f^2}\sum_{\alpha=1}^{2}\sum_{\beta=1}^{2}\int \tilde{A}_{\alpha i}^*\left(\frac{f\mathbf{u}-\mathbf{r}_d}{\lambda f},z\right)\tilde{A}_{\beta j}\left(\frac{\mathbf{u}}{\lambda},z\right)\tilde{\mu}_{\alpha\beta}\left(-\frac{2\mathbf{r}_s - \mathbf{r}_d + 2f\mathbf{u}}{2\lambda f}\right)d^2\mathbf{u}. \tag{33}$$

Above, $\mathbf{r}_s = (\mathbf{r}_1 + \mathbf{r}_2)/2$, $\mathbf{r}_d = \mathbf{r}_1 - \mathbf{r}_2$, $\boldsymbol{\rho}_s = (\boldsymbol{\rho}_1 + \boldsymbol{\rho}_2)/2$, and $\boldsymbol{\rho}_d = \boldsymbol{\rho}_1 - \boldsymbol{\rho}_2$ are the sum and difference coordinates, the tilde ˜ denotes the Fourier transform, and the vector $\mathbf{u}$ is introduced in the Fourier transform process. By letting the $\mathbf{r}_1 = \mathbf{r}_2 = \mathbf{r}$, i.e., $\mathbf{r}_s = \mathbf{r}$ and $\mathbf{r}_d = 0$ in Eq. (33), the 3×3 polarization matrix near the focal region is obtained as

$$\Phi_{ij}(\mathbf{r}, z) = \frac{1}{\lambda^2 f^2} \sum_{\alpha=1}^{2} \sum_{\beta=1}^{2} \left[\tilde{A}^*_{\alpha i}\left(-\frac{\mathbf{r}}{\lambda f}, z \right) \tilde{A}_{\beta j}\left(-\frac{\mathbf{r}}{\lambda f}, z \right) \right] \otimes \tilde{\mu}_{\alpha\beta}\left(-\frac{\mathbf{r}}{\lambda f} \right), \tag{34}$$

where $\otimes$ denotes a convolution operator, i.e., $\int A(\mathbf{u}) B(\mathbf{r} - \mathbf{u}) \mathrm{d}^2\mathbf{u} = A(\mathbf{r}) \otimes B(\mathbf{r})$ with which the integral in Eq. (33) can be converted into the convolution in Eq. (34). The polarization matrix for a tightly focused partially coherent electromagnetic Schell-model beam thus can be solved effectively with the help of fast algorithms for the Fourier transform and the convolution operation in Eq. (34). It is worth noting that the efficiency of the convolution method used here is independent of the spatial coherence width of the incident beam. Thus, it is more efficient to calculate the polarization matrix for the lowly coherent incident beam [27], compared to the pseudomode representation method developed before [34]. However, the pseudomode representation method can be used to calculate the tightly focusing properties (including one-point polarization and two-point coherence properties) for the incident beam with arbitrary coherence properties, while the convolution method is only available for calculating the one-point polarization properties for the incident beam with Schell-model coherence.

IV. SIMULATION RESULTS

In this section, we present the simulation results concerning the 3D polarization properties in the focal plane of the tightly focused partially coherent electromagnetic Schell-model beam. The incident beam is considered to be a radially polarized Gaussian Schell-model beam [35,36]. The deterministic amplitudes of such beam along x and y directions are expressed, respectively, as

$$\mathcal{A}_1(\boldsymbol{\rho}) = (\rho_x / w_0) e^{-\boldsymbol{\rho}^2 / w_0^2}, \tag{35}$$

$$\mathcal{A}_2(\boldsymbol{\rho}) = (\rho_y / w_0) e^{-\boldsymbol{\rho}^2 / w_0^2}, \tag{36}$$

and the normalized correlation functions obey

$$\mu_{\alpha\beta}(\boldsymbol{\rho}_1 - \boldsymbol{\rho}_2) = e^{-(\boldsymbol{\rho}_1 - \boldsymbol{\rho}_2)^2 / (2\delta_0^2)}, \tag{37}$$

where w_0 and δ_0 denote the beam waist and the transverse spatial coherence width, respectively. We note that the incident beam is fully polarized and it will become partially polarized and show 3D polarization properties during strong focusing due to its partial spatial coherence. In the simulation, the parameters of the focusing objective lens are taken to be NA $= 0.95$, $f = 3$ mm, and $n_t = 1$. The wavelength and the beam waist of the incident beam are $\lambda = 632.8$ nm and $w_0 = 1$ mm, respectively. The transverse spatial coherence width δ_0 varies in the simulation to show the effect of spatial coherence on the 3D polarization features.

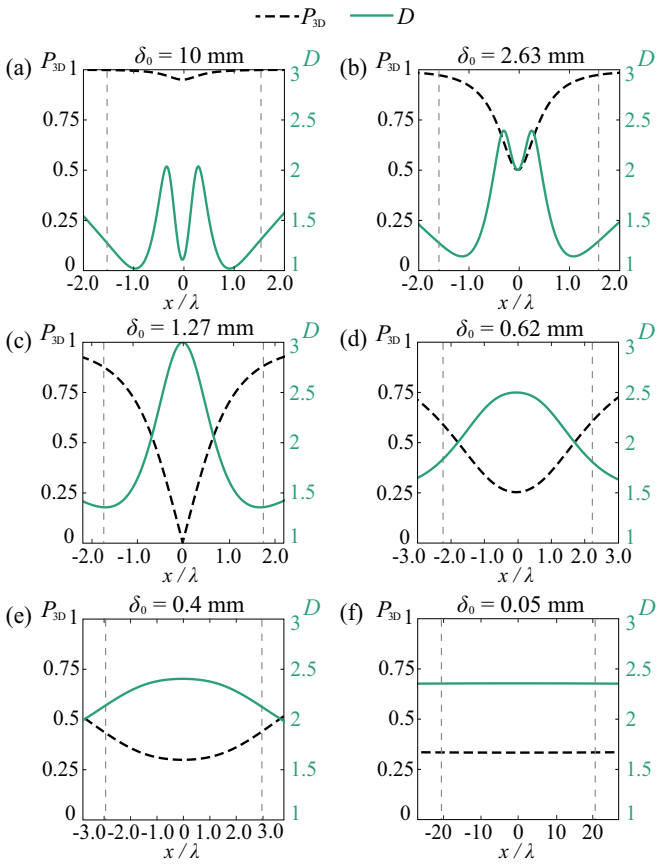

FIG. 1. Simulation results for the 3D degree of polarization P_{3D} and the polarimetric dimension D in the focal plane ($z = 0$) for a tightly focused radially polarized Gaussian Schell-model beam when the transverse spatial coherence width δ_0 is (a) 10 mm, (b) 2.63 mm, (c) 1.27 mm, (d) 0.62 mm, (e) 0.4 mm, and (f) 0.05 mm, respectively. The dashed vertical lines show the boundary of the region where the intensity is larger than 10% of its maximum value.

A. 3D degree of polarization and polarimetric dimension

We first examine the 3D degree of polarization and the polarimetric dimension of the tightly focused beam in the focal plane with the help of Eqs. (8) and (18) as well as Eq. (34). Figure 1 shows the simulation results for the spatial distributions of the 3D degree of polarization P_{3D} and the polarimetric dimension D in the focal plane ($z = 0$) for a tightly focused radially polarized Gaussian Schell-model beam whose transverse spatial coherence width δ_0 is 10, 2.63, 1.27, 0.62, 0.4, and 0.05 mm, respectively. Since the beam shows circular symmetry in a transverse plane during strong focusing, we plot only the cross line along the x direction ($y = 0$) for P_{3D} and D. The dashed vertical lines in the figures show the boundary of the area where the intensity is larger than 10% of its maximum value. At the same time, we present in Fig. 2 the focal-plane intensity distributions including the total intensity $S(\mathbf{r}, 0) = \Phi_{11}(\mathbf{r}, 0) + \Phi_{22}(\mathbf{r}, 0) + \Phi_{33}(\mathbf{r}, 0)$, the intensity for the transverse field components $S_x(\mathbf{r}, 0) + S_y(\mathbf{r}, 0) = \Phi_{11}(\mathbf{r}, 0) + \Phi_{22}(\mathbf{r}, 0)$, and the intensity

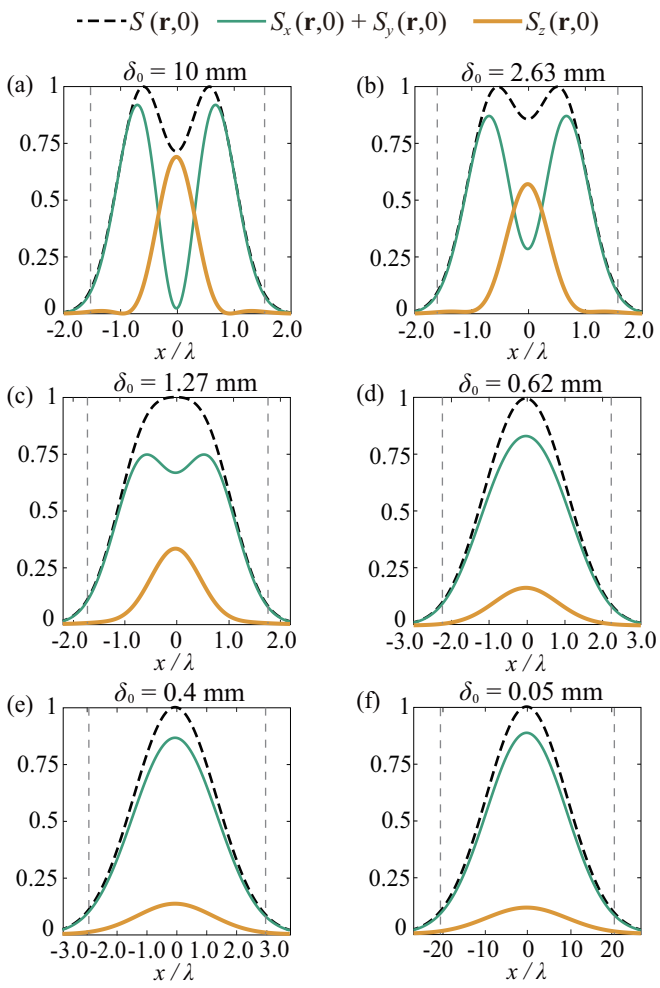

FIG. 2. Simulation results for the focal-plane intensity distributions including the total intensity $S(\mathbf{r}, 0)$, the intensity for the transverse field components $S_x(\mathbf{r}, 0) + S_y(\mathbf{r}, 0)$, and the intensity for the longitudinal field component $S_z(\mathbf{r}, 0)$ for the tightly focused radially polarized Gaussian Schell-model beam when the transverse spatial coherence width δ_0 is (a) 10 mm, (b) 2.63 mm, (c) 1.27 mm, (d) 0.62 mm, (e) 0.4 mm, and (f) 0.05 mm, respectively. The dashed vertical lines show the boundary of the region where the total intensity is larger than 10% of its maximum value.

for the longitudinal field component $S_z(\mathbf{r}, 0) = \Phi_{33}(\mathbf{r}, 0)$ for the tightly focused radially polarized Gaussian Schell-model beams with the above six spatial coherence widths.

From the simulation results in Fig. 1, we find that for the highly coherent incident beam [Fig. 1(a), $\delta_0 = 10$ mm], the field in the focal plane is effectively highly polarized with its 3D degree of polarization $P_{3D}(\mathbf{r})$ tending to unity. As a result, the focus field lacks 3D character with the polarimetric dimension bounded as $1 \leqslant D(\mathbf{r}) \leqslant 2$. It is further found that at the beam center ($\mathbf{r} = 0$), the field is nearly 1D polarized with $D \to 1$. This is because, for the highly coherent radially polarized incident beam, the transverse field in the focal plane shows a dark-hollow intensity distribution and the longitudinal field shows a bright spot as shown in Fig. 2(a). Thus, the beam at the center is strongly linearly polarized along the z direction [37]. Around the beam center, the field is elliptically polarized and becomes circularly polarized when $D(\mathbf{r}) = 2$ as both the intensities for the transverse and longitudinal fields do not vanish and the transverse and longitudinal fields are strongly correlated with a $\pi/2$ phase difference. It is found that with the further increase of the radial distance, the field becomes 1D again, and now, with a radial polarization state in the 2D transverse plane. As shown in the intensity distribution in Fig. 2(a), this is due to the vanishment of the longitudinal field.

When the spatial coherence of the incident beam decreases, i.e., the transverse spatial coherence width δ_0 changes from 10 mm to 2.63 mm, the polarimetric dimension D starts to assume values larger than 2, indicating the true 3D polarization character of the focused field. In addition, the focused field becomes partially polarized in the high-intensity region. At the beam center in the focal plane, we find that the 3D degree of polarization reduces to its smallest value ($\approx$0.5) and the polarimetric dimension $D \approx 2$. It is noted that the state at the center is not a 2D unpolarized state since the field contains three nonvanishing orthogonal components as shown in Fig. 2(b) and all these components are partially correlated. The polarization constituents of the state at the center will be discussed below in Fig. 3. Around the beam center, it is found that the degree of polarization increases, which means that the state becomes farther away from the 3D unpolarized state. However, it is counterintuitive that the polarimetric dimension D increases to the value larger than 2. One possible reason is that the 3D nonregular state appears in the polarization state of the focused field [12]. This point will be confirmed in Fig. 3 when we discuss the polarimetric nonregularity of the field. With further expanding the radial distance, the intensity of the longitudinal field component quickly vanishes, while the intensity of the transverse field component remains nonzero. As a result, the field becomes radially polarized again with polarimetric dimension tending to 1.

With the spatial coherence width of the incident beam reducing to $\delta_0 = 1.27$ mm, we find in Fig. 1(c) that the polarimetric dimension D reaches its maximum value $D = 3$ at the beam center and the corresponding 3D degree of polarization decreases to 0. The only possible state at this point is the 3D unpolarized state with the field components at this point along x, y, and z directions being completely uncorrelated and having identical intensities. As shown in Fig. 2(c), at the beam center the intensity $S_x(\mathbf{r}, 0) + S_y(\mathbf{r}, 0)$ for the transverse field components are two times of the intensity $S_z(\mathbf{r}, 0)$ for the longitudinal field component. It is also found in Fig. 1(c) that the field is essentially 3D with the polarimetric dimension $D > 2$ when the 3D degree of polarization $P_{3D} < 0.5$. In addition, we find in Fig. 1(c) that the minimum value for the polarimetric dimension increases with the decrease of the incident beam's spatial coherence. This is because the intensity distribution for the longitudinal field component expands as shown in Fig. 2(c). Thus, the polarization state along the ring where D reaches its minimum value is no longer a radial polarization state in the transverse plane as the longitudinal field component does not vanish.

When the spatial coherence of the incident beam continues to decrease, we find the minimum value for the polarimetric dimension in the significant intensity region increases since the intensity distribution for the longitudinal field component

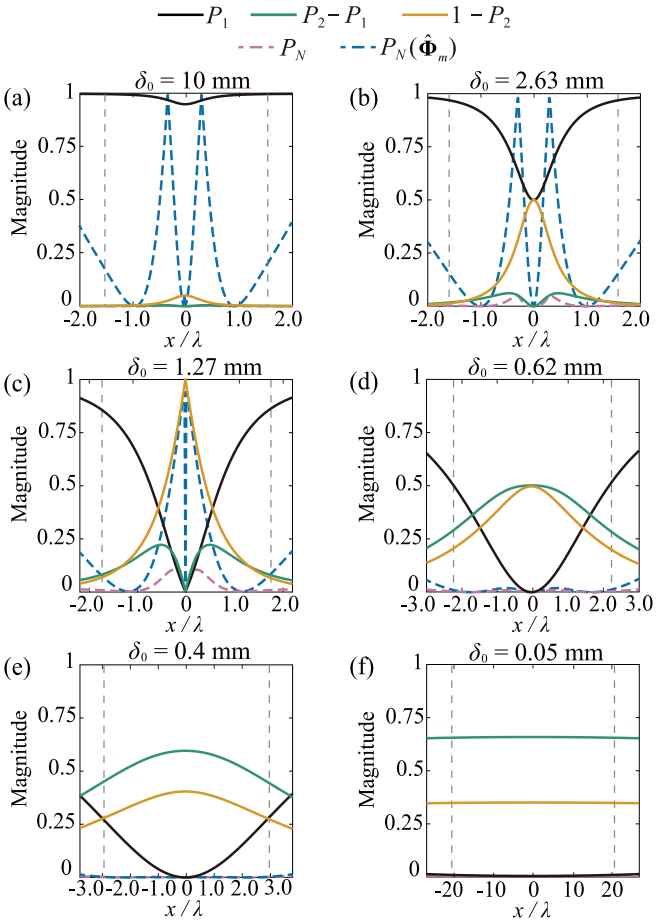

FIG. 3. Simulation results for the coefficients P_1, $P_2 - P_1$, and $1 - P_2$ in the 3D characteristic decomposition and the degrees of nonregularity $P_N(\hat{\mathbf{\Phi}}_m)$ and P_N of the middle-term state $\hat{\mathbf{\Phi}}_m$ and the whole polarization state $\mathbf{\Phi}$ for a tightly focused radially polarized Gaussian Schell-model beam in the focal plane ($z = 0$) when the transverse spatial coherence width δ_0 is (a) 10 mm, (b) 2.63 mm, (c) 1.27 mm, (d) 0.62 mm, (e) 0.4 mm, and (f) 0.05 mm, respectively. The dashed vertical lines show the boundary of the region where the intensity is larger than 10% of its maximum value.

expands further. At the same time, it is observed that the maximum value for the polarimetric dimension at the beam center decreases with the reducing of the incident beam's spatial coherence. This can be explained with the help of the intensity distributions in Fig. 2. It is found that the intensity contribution from the longitudinal field decreases with the spatial coherence. When $\delta_0 = 1.27$ mm, we show that the intensities for the longitudinal field component and the x and y field components are equal, representing an 3D intensity-isotropic unpolarized state. When $\delta_0 < 1.27$ mm, the intensity distribution becomes anisotropic with the intensity along the longitudinal direction being smaller than the intensities along x and y directions. As a result, the polarimetric dimension decreases at the beam center and the 3D degree of polarization increases. Nevertheless, the polarimetric dimension $D > 2$ still holds when the 3D degree of polarization $P_{3D} < 0.5$ as shown in Figs. 1(d) to 1(f). In Figs. 1(e) and 1(f), it is found that in all the significant intensity region the 3D degree of polarization $P_{3D} < 0.5$ and the the polarimetric dimension $D > 2$, indicating that the field is genuinely 3D in character over the whole focal domain. In the limit case $\delta_0 \ll w_0$ [Fig. 1(f), $\delta_0 = 0.05$ mm], we find the spatial distributions for the 3D degree of polarization and polarimetric dimension become nearly uniform within the high-intensity region with $P_{3D} \approx 0.33$ and $D \approx 2.35$.

B. 3D characteristic decomposition and polarimetric nonregularity

We now turn to examine the characteristic decomposition of the polarization state for the tightly focused radially polarized Gaussian Schell-model beam and find out the polarimetric structure of the 3D polarization state. The polarization state $\mathbf{\Phi}$ obtained with the convolution method is decomposed into the states $\hat{\mathbf{\Phi}}_p$, $\hat{\mathbf{\Phi}}_m$, and $\hat{\mathbf{\Phi}}_u$ with the help of the formulas introduced in Sec. II B. In Fig. 3, we display the spatial distributions for the weights P_1, $P_2 - P_1$, and $1 - P_2$ for the above three states. First of all, we find the polarization state of the tightly focused field is composed mainly by the pure state for the case when the incident beam is highly coherent [Fig. 3(a), $\delta_0 = 10$ mm], which also reflects that the focused field is highly polarized and the polarimetric dimension is bounded as $1 \leqslant D(\mathbf{r}) \leqslant 2$. With the decrease of the spatial coherence of the incident beam, the contribution of the pure state to the polarization matrix decreases as well. Meanwhile, the contributions of the middle-term state $\hat{\mathbf{\Phi}}_m$ and the 3D unpolarized state $\hat{\mathbf{\Phi}}_u$ to the polarization matrix increase. When the spatial coherence width of the incident beam decreases to $\delta_0 = 2.63$ mm [Fig. 3(b)], it is found that at the beam center the polarization matrix is composed by the pure state and the 3D unpolarized state with their weights $P_1 \approx P_2 - P_1 \approx 0.5$, indicating that the field at the center shows the true 3D character, although as shown in Fig. 1(b) that $P_{3D}(0) = 0.5$ and $D(0) = 2$. Around the beam center, the contribution from the pure state increases again and the contribution from the 3D unpolarized state decreases. Thus, the field becomes more polarized, which coincides with the result obtained in Fig. 1(b). In addition, we find that around the beam center, the contribution from $\hat{\mathbf{\Phi}}_m$ appears [see the green solid curve in Fig. 3(b)]. To show whether the state is a 3D nonregular state, we plot in Fig. 3 the degree of nonregularity for $\hat{\mathbf{\Phi}}_m$ (blue dashed curve) and for $\hat{\mathbf{\Phi}}$ (purple dashed curve) as well. It is found that $\hat{\mathbf{\Phi}}_m$ is almost perfectly nonregular with $P_N(\hat{\mathbf{\Phi}}_m) \approx 1$ on a certain ring surrounding the beam center. Thus, the 3D character of the field on this ring is determined by not only the 3D unpolarized state but also the 3D nonregular state. Therefore, we observe in Fig. 1(b) that the polarimetric dimension of the field is highest ($D > 2$) on this ring although the contribution of the 3D unpolarized state reduces, compared to the field at the beam center. We remark that for the highly coherent case, $\delta_0 = 10$ mm, the component $\hat{\mathbf{\Phi}}_m$ also shows perfectly nonregular on a certain ring surrounding the beam center. However, in this case the weight factor $P_2 - P_1$ is virtually zero. Thus, the contribution of $\hat{\mathbf{\Phi}}_m$ to the total state $\mathbf{\Phi}$ is negligible.

With the further decrease of the spatial coherence, we find in Fig. 3(c) that the field at the beam center is now composed only by the 3D unpolarized state. Thus, the 3D degree of polarization at this point vanishes and the polarimetric dimension reaches 3. Around the beam center, we find

the contribution of the 3D unpolarized state decreases, while the contributions from the pure state $\hat{\mathbf{\Phi}}_p$ and the middle-component state $\hat{\mathbf{\Phi}}_m$ increase. As a result, the field becomes more polarized and the polarimetric dimension decreases with the radial distance increasing. At the same time, it is found from the curve of the degree of nonregularity that the middle component $\hat{\mathbf{\Phi}}_m$ shows the 3D nonregular polarization state. When the spatial coherence of the incident beam decreases to $\delta_0 = 0.62$ mm, the contributions from both the 3D unpolarized state and the pure state decrease everywhere, while the contribution from $\hat{\mathbf{\Phi}}_m$ increases. The field at the beam center is now contributed to equally by $\hat{\mathbf{\Phi}}_m$ and $\hat{\mathbf{\Phi}}_u$ with $P_2 - P_1 = 1 - P_2 = 0.5$. In addition, at the beam center $\hat{\mathbf{\Phi}}_m$ is a regular 2D unpolarized state with $P_N(\hat{\mathbf{\Phi}}_m) = 0$ at the beam center. Thus, the field at the beam center in this case is composed by a 2D unpolarized state and a 3D unpolarized state with identical weights. The 3D degree of polarization is therefore fixed at $P_{3D}(0) = 0.25$ and the polarimetric dimension is fixed at $D(0) = 2.5$. With the increase of the radial distance, the contributions from $\hat{\mathbf{\Phi}}_m$ and $\hat{\mathbf{\Phi}}_u$ decrease, while that from the pure state $\hat{\mathbf{\Phi}}_p$ increases. As a result, the 3D degree of polarization increases and the polarimetric dimension decreases. However, as shown in Fig. 3(d) the field in the focal plane is always partially polarized in the high-intensity region since the contributions from both $\hat{\mathbf{\Phi}}_m$ and $\hat{\mathbf{\Phi}}_u$ are still significant at the edge of the high-intensity region.

When the spatial coherence width decreases to $\delta_0 = 0.4$ mm, we find the contribution from $\hat{\mathbf{\Phi}}_m$ further increases, while the contributions from $\hat{\mathbf{\Phi}}_p$ and $\hat{\mathbf{\Phi}}_u$ decrease. In the high-intensity region, both the contributions from $\hat{\mathbf{\Phi}}_m$ and $\hat{\mathbf{\Phi}}_u$ become dominant. Thus, the 3D degree of polarization becomes less than 0.5 and the polarimetric dimension $D > 2$ in the high-intensity region. When the spatial coherence width decreases to a limited case, i.e., $\delta_0 = 0.05$ mm, it is found that the polarization state is composed only by $\hat{\mathbf{\Phi}}_m$ and $\hat{\mathbf{\Phi}}_u$ with their weights distributed uniformly in the space.

Throughout the evolution of the incident beam's spatial coherence, it is observed that the contribution from the pure state decreases from 1 to 0 with the incident beam becoming from highly coherent to highly incoherent. In the mean time, the contribution from the 3D unpolarized state first increases from 0, then decreases after reaching the maximum at $\delta_0 = 1.27$ mm, and finally tends to 0.35 at the low coherence limit [Fig. 3(f)]. The contribution from the middle-term state, on the other hand, increases monotonously with the decrease of δ_0 and reaches 65% at $\delta_0 = 0.05$ mm. It is remarkable that, although the contribution from the middle-term state $\hat{\mathbf{\Phi}}_m$ increases with the decrease of the spatial coherence, we find the degree of nonregularity $P_N(\hat{\mathbf{\Phi}}_m)$ decreases as well. Thus, the field gradually becomes regular with the decrease of the spatial coherence as shown in Figs. 3(d), 3(e), and 3(f).

C. Spin structure

From the above simulation results, we show that the focused field is composed mainly by pure polarization state for the highly coherent incident beam, while for the virtually incoherent incident beam, the focused field is composed by the 2D unpolarized state and the 3D unpolarized state. For the partially coherent incident beam with the spatial coherence width δ_0 compared to the beam waist w_0, the tightly focused field is composed by all three constituents in the polarization matrix's 3D characteristic decomposition. In addition, the middle-term state in the characteristic decomposition shows the 3D nonregularity. Therefore, we can predict that the total spin density is contributed by the pure state only for the highly coherent case, while it is contributed by both the pure state and the 3D nonregular polarization state for the partially coherent case. For the incoherent incident beam, the focused field contains no spin since the field is composed only by the 2D and 3D unpolarized states.

In Fig. 4, we present the simulation results for the spin density vectors $\mathbf{s}_p$ and $\mathbf{s}_m$ as well as their x, y, and z components for the tightly focused radially polarized Gaussian Schell-model beams with the initial spatial coherence widths $\delta_0 = 2.63$ mm, 1.27 mm, and 0.62 mm. It is found in Fig. 4(a) that for the relatively high coherence case, the total spin is composed mainly by the spin density vector $\mathbf{s}_p$ for the pure state in the significant-intensity region. This is because the contribution from the middle-term state $\hat{\mathbf{\Phi}}_m$ to the total polarization matrix is small at $\delta_0 = 2.63$ mm, although its degree of nonregularity is quite high. In addition, we find in the spatial distributions for the spin density components that both $\mathbf{s}_p$ and $\mathbf{s}_m$ show the pure transverse spin distribution with the longitudinal spin components s_{pz} and s_{mz} vanishing. Physically, the transverse spin density is induced due to the out-of-phase longitudinal field component generated during light strong focusing [38,39]. The longitudinal spin density is zero because the two orthogonal field components in the transverse plane are always in phase. Furthermore, it is found that the transverse spin density vectors show the azimuthal vortex distribution. This is due to the circularly symmetric spatial coherence and radial polarization state of the incident beam.

With the decrease of the spatial coherence, we find the contribution of $\mathbf{s}_m$ to the total spin increases. When the spatial coherence width $\delta_0 = 1.27$ mm, the contribution from the spin $\mathbf{s}_p$ for the pure state is still dominant. However, when the spatial coherence width $\delta_0 = 0.62$ mm, the spin $\mathbf{s}_m$ for the middle-term state becomes dominant in the center region [see the light green zone in Fig. 4(c)]. From the spatial distributions of the spin density components, it is found that, with the decrease of the spatial coherence, the spatial distributions for the spin density vectors remain almost unchanged. However, we remark that with the decrease of the spatial coherence of the incident beam, the magnitude of the spin density of the tightly focused field decreases as well. This can be understood in the following way. Based on the vectorial diffraction theory, the field at an arbitrary position in the focal plane is determined by the contributions from the fields at all the positions in the input plane. For a radially polarized incident beam, the input fields at different positions, in general, will create the fields with different polarization states at a same point in the focal plane. Moreover, due to the decreased coherence between the fields at different positions in the input plane, the correlation among the transverse and longitudinal field components in the focal plane will become weaker. As a result, the magnitude of the spin density decreases with the spatial coherence of the incident beam. In the limit case when

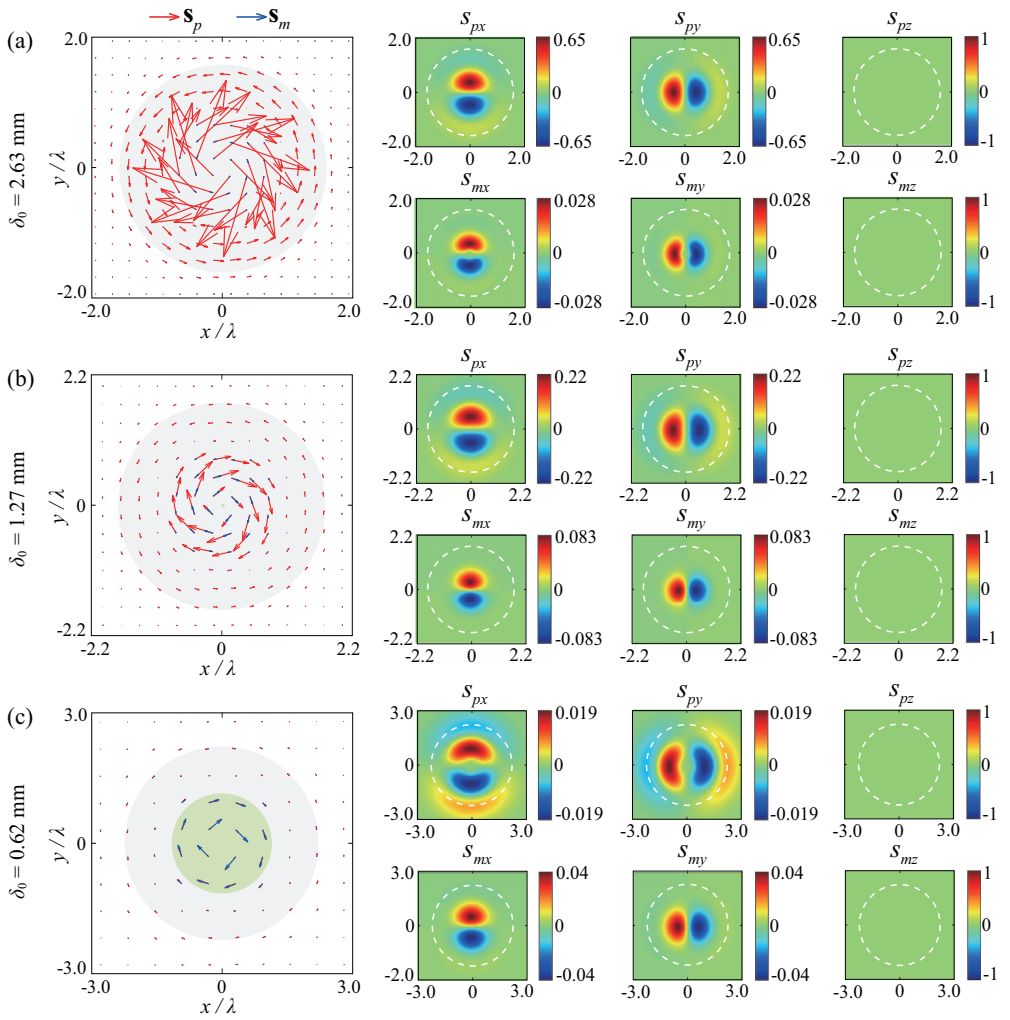

FIG. 4. Simulation results for the spin density vectors $\mathbf{s}_p = (s_{px}, s_{py}, s_{pz})$ and $\mathbf{s}_m = (s_{mx}, s_{my}, s_{mz})$ and their x, y, and z components for the tightly focused radially polarized Gaussian Schell-model beam in the focal plane ($z = 0$) when the transverse spatial coherence width δ_0 is (a) 2.63 mm, (b) 1.27 mm, and (c) 0.62 mm, respectively. Inside the dark gray areas in the first column and inside the white dashed rings in the last three columns, the intensity is larger than 10% of its maximum value. The light green zone in the first column of (c) corresponds to the regions where $|\mathbf{s}_m| > |\mathbf{s}_p|$.

the incident beam is incoherent, the spin density in the focal plane becomes zero since the focused field is now composed only of the 2D and 3D unpolarized states.

V. CONCLUSIONS

In summary, we studied the 3D polarization properties of a tightly focused electromagnetic partially coherent Gaussian Schell-model beam by examining the 3D degree of polarization, polarimetric dimension, and polarimetric structure of its 3×3 polarization matrix. The 3D polarimetric structure was obtained via the characteristic decomposition, with which the polarization matrix is decomposed as an incoherent superposition of a pure state, a middle-term state, and a 3D unpolarized state. We also studied the polarimetric nonregularity and the associated spin structure of the 3D polarization state in the focused field with such a decomposition. The 3×3 polarization matrix of the tightly focused partially coherent Schell-model beam was computed with a fast convolution method operated in the generalized (two-point) Richards–Wolf's vectorial integral.

It was demonstrated that the highly focused field showed the genuine 3D partially polarized state even though the incident beam is fully radially polarized. We showed that the 3D polarization state induced in the focal plane is due to the reduced spatial coherence in the incident beam. By examining the effect of the incident beam's spatial coherence width on the focal-plane 3D polarization characters, it was found that with the decrease of the initial spatial coherence, the contribution to the polarization matrix from the pure state in the characteristic decomposition decreases and from the middle-component state increases, while the contribution from the 3D unpolarized state first increases and then decreases after reaching the maximum. In the limiting case when the incident beam is spatially incoherent, it was found that the focused field is composed only by the middle-term state and the 3D unpolarized state. The simulation results for the polarimetric nonregularity showed that the weight and the degree of

nonregularity of the middle-term state reduce, respectively, with the increase and decrease of the spatial coherence. Therefore, the focused field created by the radially polarized Gaussian Schell-model beam is in the 3D nonregular state only when the spatial coherence width is compared to the initial beam's waist.

In addition, we demonstrated that the spin density vector in the focused field, induced by the generation of the out-of-phase longitudinal field component during tight focusing of the radially polarized beam, is contributed by the spins from both the pure state and the middle-term state when the field is in the 3D nonregular state. It was found that the total spin density vector is contributed mainly to by the pure state for the highly coherent incident beam, while with the decrease of the spatial coherence, the contribution to the total spin from the middle-term state increases and can even be dominant when the spatial coherence width is smaller than the initial beam's waist. We observed that the magnitude of the total spin, however, decreases with the spatial coherence of the incident beam as the correlation between the transverse and longitudinal field components in the focal plane becomes weaker and the middle-term state becomes more regular. In the limiting case when the incident beam is spatially incoherent, the focused field lacks spin since the field is now composed only by the 2D and 3D unpolarized states. We expect that our findings could be useful in shaping the 3D polarization state and spin structure of light on nanoscale with modulating the degree of spatial coherence of light.

ACKNOWLEDGMENTS

This research was supported by the National Natural Science Foundation of China (NSFC) (11974218, 11904247, 12192254, 12274310, 92250304), the National Key Research and Development Project of China (2019YFA0705000, 2022YFA1404800), and the Local Science and Technology Development Project of the Central Government (YDZX20203700001766).

[1] D. H. Goldstein, *Polarized Light*, 3rd ed. (CRC Press, Boca Raton, 2011).
[2] L. Mandel and E. Wolf, *Optical Coherence and Quantum Optics* (Cambridge University, Cambridge, 1995).
[3] C. Brosseau, *Fundamentals of Polarized Light: A Statistical Optics Approach* (Wiley, New York, 1998).
[4] L. Novotny and B. Hecht, *Principles of Nano-Optics*, 2nd ed. (Cambridge University, Cambridge, 2012).
[5] J. J. Gil and R. Ossikovski, *Polarized Light and the Mueller Matrix Approach* (CRC Press, Boca Raton, 2016).
[6] M. Born and E. Wolf, *Principles of Optics* (Cambridge University Press, Cambridge, 1999).
[7] A. Norrman, A. T. Friberg, J. J. Gil, and T. Setälä, Dimensionality of random light fields, J. Eur. Opt. Soc.- Rapid Publ. **13**, 36 (2017).
[8] J. J. Gil, Polarimetric characterization of light and media, Eur. Phys. J. Appl. Phys. **40**, 1 (2007).
[9] J. Ellis, A. Dogariu, S. Ponomarenko, and E. Wolf, Degree of polarization of statistically stationary electromagnetic fields, Opt. Commun. **248**, 333 (2005).
[10] J. Ellis and A. Dogariu, On the degree of polarization of random electromagnetic fields, Opt. Commun. **253**, 257 (2005).
[11] J. J. Gil, Interpretation of the coherency matrix for three-dimensional polarization states, Phys. Rev. A **90**, 043858 (2014).
[12] J. J. Gil, A. T. Friberg, T. Setälä, and I. San José, Structure of polarimetric purity of three-dimensional polarization states, Phys. Rev. A **95**, 053856 (2017).
[13] J. J. Gil, A. Norrman, A. T. Friberg, and T. Setälä, Nonregularity of three-dimensional polarization states, Opt. Lett. **43**, 4611 (2018).
[14] L. Allen, S. M. Barnett, and M. J. Padgett, *Optical Angular Momentum* (IOP Publishing, Boca Raton, 2003).
[15] K. Y. Bliokh and F. Nori, Transverse and longitudinal angular momenta of light, Phys. Rep. **592**, 1 (2015).
[16] A. Aiello, P. Banzer, M. Neugebauer, and G. Leuchs, From transverse angular momentum to photonic wheels, Nat. Photonics **9**, 789 (2015).
[17] P. Shi, L. Du, and X. Yuan, Spin photonics: From transverse spin to photonic skyrmions, Nanophotonics **10**, 3927 (2021).
[18] J. Chen, C. Wan, and Q. Zhan, Engineering photonic angular momentum with structured light: A review, Adv. Photonics **3**, 064001 (2021).
[19] J. J. Gil, A. T. Friberg, A. Norrman, and T. Setälä, Effect of polarimetric nonregularity on the spin of three-dimensional polarization states, New J. Phys. **23**, 063059 (2021).
[20] Y. Chen, A. Norrman, S. A. Ponomarenko, and A. T. Friberg, Optical coherence and electromagnetic surface waves, Prog. Opt. **65**, 105 (2020).
[21] A. Norrman, J. J. Gil, A. T. Friberg, and T. Setälä, Polarimetric nonregularity of evanescent waves, Opt. Lett. **44**, 215 (2019).
[22] J. S. Eismann, L. H. Nicholls, D. J. Roth, M. A. Alonso, P. Banzer, F. J. Rodriguez-Fortuño, A. V. Zayats, F. Nori, and K. Y. Bliokh, Transverse spinning of unpolarized light, Nat. Photonics **15**, 156 (2021).
[23] Y. Chen, F. Wang, Z. Dong, Y. Cai, A. Norrman, J. J. Gil, A. T. Friberg, and T. Setälä, Polarimetric dimension and nonregularity of tightly focused light beams, Phys. Rev. A **101**, 053825 (2020).
[24] Y. Chen, F. Wang, Z. Dong, Y. Cai, A. Norrman, J. J. Gil, A. T. Friberg, and T. Setälä, Structure of transverse spin in focused random light, Phys. Rev. A **104**, 013516 (2021).
[25] Z. Chen, L. Hua, and J. Pu, Tight focusing of light beams: effect of polarization, phase, and coherence, Prog. Opt. **57**, 219 (2012).
[26] Y. Dong, F. Feng, Y. Chen, C. Zhao, and Y. Cai, Statistical properties of a nonparaxial cylindrical vector partially coherent field in free space, Opt. Express **20**, 15908 (2012).
[27] M. Aviñoá, R. Martínez-Herrero, and A. Carnicer, Efficient calculation of highly focused electromagnetic Schell-model beams, Opt. Express **29**, 26220 (2021).
[28] A. T. Friberg and T. Setälä, Electromagnetic theory of optical coherence (invited), J. Opt. Soc. Am. A **33**, 2431 (2016).
[29] M. R. Dennis, Geometric interpretation of the three-

dimensional coherence matrix for nonparaxial polarization, J. Opt. A: Pure Appl. Opt. **6**, S26 (2004).

[30] J. J. Gil, Intrinsic Stokes parameters for 3D and 2D polarization states, J. Eur. Opt. Soc.- Rapid Publ. **10**, 15054 (2015).

[31] T. Setälä, A. Shevchenko, M. Kaivola, and A. T. Friberg, Degree of polarization for optical near fields, Phys. Rev. E **66**, 016615 (2002).

[32] J. J. Gil, A. Norrman, A. T. Friberg, and T. Setälä, Polarimetric purity and the concept of degree of polarization, Phys. Rev. A **97**, 023838 (2018).

[33] B. Richards and E. Wolf, Electromagnetic diffraction in optical system II. Structure of the image field in an aplanatic system, Proc. R. Soc. London A **253**, 358 (1959).

[34] R. Tong, Z. Dong, Y. Chen, F. Wang, Y. Cai, and T. Setälä, Fast calculation of tightly focused random electromagnetic beams: Controlling the focal field by spatial coherence, Opt. Express **28**, 9713 (2020).

[35] Y. Dong, Y. Cai, C. Zhao, and M. Yao, Statistics properties of a cylindrical vector partially coherent beam, Opt. Express **19**, 5979 (2011).

[36] F. Wang, Y. Cai, Y. Dong, and O. Korotkova, Experimental generation of a radially polarized beam with controllable spatial coherence, Appl. Phys. Lett. **100**, 051108 (2012).

[37] K. S. Youngworth and T. G. Brown, Focusing of high numerical aperture cylindrical-vector beams, Opt. Express **7**, 77 (2000).

[38] M. Neugebauer, T. Bauer, A. Aiello, and P. Banzer, Measuring the Transverse Spin Density of Light, Phys. Rev. Lett. **114**, 063901 (2015).

[39] M. Neugebauer, J. S. Eismann, T. Bauer, and P. Banzer, Magnetic and Electric Transverse Spin Density of Spatially Confined Light, Phys. Rev. X **8**, 021042 (2018).